AIP | Journal of Applied Physics

Thermocyclic stability of candidate Seebeck coefficient standard reference materials at high temperature

Joshua Martin, Winnie Wong-Ng, Thierry Caillat, I. Yonenaga, and Martin L. Green

Citation: Journal of Applied Physics **115**, 193501 (2014); doi: 10.1063/1.4876909
View online: http://dx.doi.org/10.1063/1.4876909
View Table of Contents: http://scitation.aip.org/content/aip/journal/jap/115/19?ver=pdfcov
Published by the AIP Publishing

Thermocyclic stability of candidate Seebeck coefficient standard reference materials at high temperature

Joshua Martin,[1,a)] Winnie Wong-Ng,[1] Thierry Caillat,[2] I. Yonenaga,[3] and Martin L. Green[1]
[1]*Material Measurement Laboratory, National Institute of Standards and Technology, Gaithersburg, Maryland 20899, USA*
[2]*Jet Propulsion Laboratory, California Institute of Technology, Pasadena, California 91109, USA*
[3]*Institute for Materials Research, Tohoku University, Sendai 980-8577, Japan*

(Received 27 March 2014; accepted 4 May 2014; published online 20 May 2014)

The Seebeck coefficient is the most widely measured property specific to thermoelectric materials. There is currently no consensus on measurement protocols, and researchers employ a variety of techniques to measure the Seebeck coefficient. The implementation of standardized measurement protocols and the use of reliable Seebeck Coefficient Standard Reference Materials (SRMs®) will allow the accurate interlaboratory comparison and validation of materials data, thereby accelerating the development and commercialization of more efficient thermoelectric materials and devices. To enable members of the thermoelectric materials community the means to calibrate Seebeck coefficient measurement equipment, NIST certified SRM® 3451 "Low Temperature Seebeck Coefficient Standard (10 K to 390 K)". Due to different practical requirements in instrumentation, sample contact methodology, and thermal stability, a complementary SRM® is required for the high temperature regime (300 K to 900 K). The principal requirement of a SRM® for the Seebeck coefficient at high temperature is thermocyclic stability. We therefore characterized the thermocyclic behavior of the Seebeck coefficient for a series of candidate materials: constantan, p-type single crystal SiGe, and p-type polycrystalline SiGe, by measuring the temperature dependence of the Seebeck coefficient as a function of 10 sequential thermal cycles, between 300 K and 900 K. We employed multiple regression analysis to interpolate and analyze the thermocyclic variability in the measurement curves. © *2014 AIP Publishing LLC*. [http://dx.doi.org/10.1063/1.4876909]

INTRODUCTION

The Seebeck coefficient, the proportionality constant that quantifies the thermoelectric conversion of an applied temperature difference into an electric potential, is an essential indicator of conversion efficiency and the most widely measured property specific to thermoelectric materials.[1,2] Materials that exhibit a large Seebeck coefficient, in addition to high electrical conductivity and low thermal conductivity, are considered candidates for use in thermoelectric applications. These applications include waste heat recovery in engines for automotive, aerospace, and military applications, and solid-state refrigeration for consumer products and microelectronics. There is currently no consensus on measurement protocols, and researchers use a variety of techniques and contact arrangements to measure the Seebeck coefficient, resulting in conflicting data that hinder the commercialization of these energy-critical materials.[3,4] In addition, the systems currently being used for measurement of the Seebeck coefficient at high temperature include both commercial and custom built systems. We have recently completed a comprehensive experimental study to elucidate the influence of these factors in the measurement of the Seebeck coefficient at high temperature and to identify standard testing protocols.[5] The implementation of standardized measurement protocols and the use of reliable Seebeck Coefficient Standard Reference Materials® (SRMs) will allow the accurate interlaboratory comparison and validation of materials data, thereby accelerating the development and commercialization of new and efficient thermoelectric materials and devices. Thermoelectric devices will have enhanced performance and shorter, less costly development cycles.

To provide the thermoelectric materials community the means to calibrate Seebeck coefficient measurement equipment for bulk materials, NIST (National Institute of Standards and Technology) certified and released for purchase in late 2011 SRM® 3451, "Low Temperature Seebeck Coefficient Standard (10 K to 390 K)".[6] Seebeck coefficient measurements are generally divided into the low (<300 K) or the high (>300 K) temperature regime, due to different practical requirements in both instrumentation and sample contact methodology. Following on the success of SRM® 3451, the Materials Measurement Science Division of NIST is currently developing a complementary high temperature Seebeck coefficient SRM® for the temperature regime 300 K to 900 K.

The material requirements for the high temperature Seebeck coefficient SRM include: long term chemical and transport property stability at high temperature after repeated thermal cycles over a broad temperature range; homogeneity in batch production; reasonable production availability and development, production, and materials costs; moderately large absolute Seebeck coefficient values (≈40 μV/K to 200 μV/K), moderate to low thermal conductivity (for thermal gradient formation power requirements), and moderate to high

a)joshua.martin@nist.gov

electrical conductivity, over a meaningfully broad portion of the high temperature regime; the ability to be shaped into the specified geometry; and proven commercial history without serious long term instability under ambient conditions, with minimal environmental concerns (should be environmentally friendly and non-toxic). Additionally, it may be advantageous to select a material that is a viable candidate for other thermoelectric-related SRMs, for other temperature regimes, or for other sample geometries such as thin film.

To determine which materials (and prismatic dimension preference) are most appropriate for the high temperature Seebeck SRM, we have performed a literature search and collected opinions from community experts. Accordingly, we have distributed questionnaires and have held panel discussions during several international conferences. The three most promising candidates are (no particular order): (1) a metal alloy: Constantan® (nominally Cu 55%–Ni 45%), and (2) a semiconductor: p-type single crystal SiGe, and (3) another semiconductor: p-type polycrystalline SiGe. Constantan displays moderate Seebeck coefficient values ($\approx 40\,\mu$V/K at 300 K) but very high electrical conductivity and high thermal conductivity. Silicon germanium alloys are well studied, high temperature thermoelectric materials with reasonably high Seebeck coefficient values ($\approx 100\,\mu$V/K to $400\,\mu$V/K at 300 K, depending on dopant concentration), high electrical conductivity, and low thermal conductivity. Constantan was obtained from Goodfellow[7] in annealed 4.0 mm diameter rod form, and was machined into prismatic dimensions $2.5 \times 2.5 \times 14\,\text{mm}^3$; p-type single crystal $Si_{90}Ge_{10}$ (SC-$Si_{90}Ge_{10}$) was prepared by a Czochralski method[8] and cut into the same prismatic dimensions using an abrasive slurry wire saw; and p-type polycrystalline $Si_{80}Ge_{20}$ (poly-$Si_{80}Ge_{20}$) was obtained from JPL (Jet Propulsion Laboratory) (also cut using a wire saw to $2.5 \times 3 \times 14\,\text{mm}^3$).

While most of the stated material requirements for the high temperature Seebeck coefficient SRM are readily discoverable, the thermocyclic stability is less characterized. Repeatedly heating a material to high temperature can result in changes to the grain structure, surface oxidation state, composition homogeneity, and dopant homogeneity through migration or precipitation, and thereby perturb the Seebeck coefficient. Although constantan is used in thermoelectric thermometry applications at high temperature, there is very little data on the long-term stability of these alloys,[9] and we could not identify any reliable data on the effect of short-term thermal cycling on the alloy itself (i.e., decoupled from the thermocouple data). For the silicon-germanium alloys, the solid solubilities of the dopants exhibit temperature dependent retrograde characteristics.[10] When the concentration of dopant in the solid solution exceeds the solubility limit at a specific temperature, the dopant can precipitate out of solution. The kinetics of precipitation in silicon-germanium alloys can be described using the diffusion-limited Lifshitz and Slyozov dopant precipitation model.[11] Accordingly, these effects are a function of time and temperature, and cumulative and may therefore be detrimental to the thermocyclic stability. Precipitation effects have been investigated by a number of researchers for both n- (phosphorus-doped) and p-type (boron-doped) silicon-germanium alloys.[10,12–15] Since the diffusion coefficient for phosphorus in Ge is larger than that of boron ($\approx$100 times at 1000 K),[10] and the activation energy smaller, n-type dopants precipitate at significantly lower annealing temperatures. For the p-type materials, the Seebeck coefficient has been measured as stable under isothermal annealing for 39 210 h below 875 K ($Si_{75}Ge_{25}$),[12] for 1500 h below 925 K ($Si_{78}Ge_{22}$),[13] and for 100 h at 1000 K ($Si_{63.5}Ge_{36.5}$).[10] We note that dopant precipitation is largely reversible by quenching after a brief 1300 K isothermal anneal.[14] However, the 1300 K anneal imposes an impractical burden for a commercial reference material. Further, there are no available data that indicate the stability of these silicon-germanium alloys as a function of non-isothermal annealing, as would be the case for repeated calibration measurements using the SRM. We have therefore conducted thermocyclic Seebeck coefficient measurements to characterize the stability of each candidate material, between 300 K and 900 K, for a series of 10 sequential thermal cycles.

EXPERIMENTAL

To realize the accuracy requirement for SRM development and certification, we designed and constructed a fully custom high temperature thermoelectric measurement apparatus that enables the unprecedented direct comparison of multiple probe arrangements, techniques, and sample geometries. Reference 16 comprehensively describes the primary instrumentation components, measurement capabilities, and design innovations that culminate in extremely low (and deterministic) measurement uncertainty. For thermocyclic stability studies, Seebeck coefficient measurements were conducted under high vacuum following a triple helium gas purge cycle. The Seebeck coefficients were measured between 300 K and 900 K. The maximum sample temperature was 900 K to minimize dopant precipitation. The entire measurement procedure was repeated 10 times sequentially for each sample using the same mounting and contacts (i.e., the samples were not removed/remounted between cycles).

Measurement of the relative Seebeck coefficient requires a minimum of three voltage measurements: one for the thermoelectric voltage ΔV and one each for the hot and cold thermocouple voltage for T_2 and T_1, respectively, that determine the temperature difference ΔT. Acquisition protocols for these parameters adhere to the following criteria, defined previously[3] as (1) the measurement of the voltage and temperature at the same locations and at the same time; (2) contact interfaces with the sample that are Ohmic and isothermal; and (3) the acquisition of small voltages with minimal extraneous contributions. The measured Seebeck coefficient S_{ab} is explicitly relative and requires the correction $S_{ab} = S_b - S_a$, where S_b is the contribution of the second conductor (platinum), to obtain S_a, the Seebeck coefficient of the sample (hereafter referred to as S). Using the differential method, a small thermal gradient ΔT was applied to the sample at an average temperature of interest $T_o = (T_1 + T_2)/2$, where $T_1 = T_o - \Delta T/2$, and $T_2 = T_o + \Delta T/2$. Here, $S = \Delta V/\Delta T$, where ΔV is the electric potential, and $\Delta T = T_2 - T_1$ is the applied temperature difference. The maximum temperature difference was between $0.001T_o$ and $0.02T_o$. We applied an increasing heat flux wherein the

voltage and temperature difference were simultaneously recorded in 5 s intervals with gradient heating rates between 5 mK/s and 50 mK/s. The Seebeck coefficient was then calculated as the slope of the unconstrained linear fit of multiple electric potential/temperature difference data points $\{(\Delta T, \Delta V)\}$. This avoids the assumption that the experimental data are collinear with the ordinate ($V=0$, $\Delta T=0$) and eliminates extraneous voltage offsets. However, thermal offsets cannot be eliminated using this technique.

We have previously demonstrated experimentally that the contact geometry, dependent on the thermal interface, is the primary limit to high accuracy, while the measurement technique, under ideal conditions, has little influence on the measured Seebeck coefficient.[5] The measurement of surface temperature by contact (a common high temperature design) is influenced by intrinsic thermal errors. Application of a sensor to the surface of the sample modifies the thermal interaction of the contacted surface with the environment, inducing a parasitic perturbation of the local temperature field. This error is larger for the 4-probe arrangement.[5] Therefore, we selected the 2-probe contact geometry for these thermal cycling experiments.

DATA ANALYSIS AND DISCUSSION

The temperature dependence of the raw Seebeck coefficient data for each of the selected candidate materials is shown in Figure 1. The room temperature (≈295 K) Seebeck coefficients measured during each of the first thermal cycles are $-29.67\,\mu$V/K, $445.66\,\mu$V/K, and $118.47\,\mu$V/K, for the constantan, SC-$Si_{90}Ge_{10}$, and poly-$Si_{80}Ge_{20}$ samples, respectively. The Seebeck coefficients for each sample appear to be generally consistent throughout the 10 sequential thermal cycles. However, statistical analyses are required to meaningfully compare the relative performance of each sample.

We employed multiple regression analysis using parametric models to interpolate and analyze the thermocyclic variability in the measurement curves that were sampled at different base temperatures. We first defined a consensus mean curve for the data set of individual measurement curves. Instead of using the mean of fitted regression coefficients for the measurement curve of each thermal cycle, we used an all

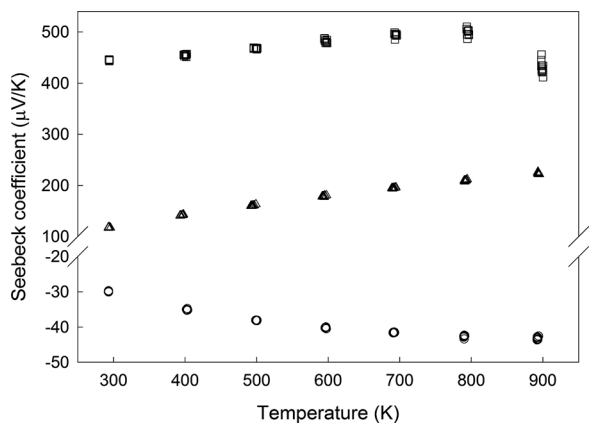

FIG. 1. The measured Seebeck coefficient as a function of temperature for constantan (open circles), SC-$Si_{90}Ge_{10}$ (open squares), and poly-$Si_{80}Ge_{20}$ (open triangles) for 10 thermal cycles each.

data regression approach.[17] A single parametric model was fit to the complete 10 cycle data set for a given sample

$$S_m(T) = S_A + \sum_{i=1}^{n} a_i T^i \left(1 - \frac{A}{T}\right)^i, \quad (1)$$

where $S_m(T)$ is the interpolated value of the Seebeck coefficient and A is the temperature around which the polynomial is expanded ($295\,\mathrm{K} \le A \le 900\,\mathrm{K}$). This form allows physical interpretation for the units of the coefficients: μV/K for S_A and $\mu\mathrm{V/K}^{i+1}$ for each coefficient a_i. For constantan and poly-$Si_{80}Ge_{20}$, $n=2$; for SC-$Si_{90}Ge_{10}$, $n=5$, selected to yield the best fit to the data as determined by a coefficient of determination, R^2. The parametric model was then applied to the measured data for each individual thermal cycle to compute a set of interpolated curves having specified base temperatures. To determine the distribution of the data, we computed the pointwise variance $v(T)$ as the mean of the squares of deviations of each curve from the consensus mean curve $S_m(T)$ (this can be smoothed by applying a spline regression). The confidence band for the consensus mean curve is then $S_m(T) = \pm\, k\sqrt{v(T)}$ with $k=2$ for a pointwise 95% confidence interval.

Uncertainty analysis was conducted in accordance with recommendations contained in the ISO Guide to the Expression of Uncertainty in Measurement[18] and the procedures and policies outlined in NIST Technical Note #1297.[19] Uncertainties associated with the results of the Seebeck coefficient measurements were categorized as components that can be evaluated statistically (type A) and those that cannot (type B). Type A uncertainties were obtained as the square root of the variance function $v(T)$ for the data set of each material. Type B uncertainties are systematic in origin and primarily derive from instrumentation, data acquisition, and/or calibration errors. For type B uncertainty, only those systematic uncertainties arising from the measurement of the hot and cold thermocouples and the electric potential were considered. We note that the uncertainty component derived from the thermoelectric voltage was negligible compared to the temperature components and was therefore ignored. At 295 K, the voltage reading for an R-type thermocouple is $\approx 10\,\mu$V and the standard uncertainty is 0.4%. In addition, the thermocouple manufacturer's quoted accuracy is 0.25 K. Therefore, the combined standard measurement uncertainty for each thermocouple is 0.48% T. The uncertainty in ΔT is $(0.48^2 + 0.48^2)^{1/2}\% = 0.68\%$. Consequently, the Seebeck coefficient, computed as the least square estimate of the slope based on the data $\{(\Delta T, \Delta V)\}$, where the linear regressions approximate the voltage and temperature difference data better than 4σ, has the same 0.68% uncertainty. There was also an uncertainty arising from the average sample temperature measurement, T, given by the compound average of the collection of sample temperature values obtained for each ΔT and ΔV pair, where each sample temperature was calculated as the simple average of the hot and cold thermometer measurements. The uncertainty for the average base temperature was computed easily in terms of uncertainties for individual temperatures, i.e., $[(0.48/2)^2 + (0.48/2)^2]^{1/2}\% = 0.34\%$. The Seebeck coefficient uncertainty component associated with

this average base temperature uncertainty was then calculated as $(0.0034)T|S'_m(T)|$, where $S'_m(T)$ is the derivative of the parameterized consensus mean (Eq. (1)). These are combined for the total type B uncertainty (e.g., the type B relative uncertainty is ≈0.7% in the stated temperature range). The type A and B standard uncertainty components were then combined using the RSS method (root sum of squares) for a total standard uncertainty, u_c. The total expanded uncertainty for the Seebeck coefficient measurement curves is then $S_m(T) = \pm ku_c$ with $k = 2$ for a 95% confidence band.

Figure 2(a) plots the Seebeck coefficient for constantan as a function of temperature for the complete set of 10 cycles, including the consensus mean curve, the type A expanded confidence intervals, and the total expanded uncertainty confidence bands. To characterize the stability of the material, we first compare the distribution of the data (the type A component, obtained as the square root of the variance function $v(T)$ for the data set) with the type B component. Figure 2(b) plots the type A and type B uncertainty components (labeled as σ_A and σ_B, respectively) as a function of temperature. Throughout the temperature range, the type B uncertainty component is <0.3 μV/K (≈0.7% relative uncertainty). In comparison, the type A uncertainty component is smaller at lower temperature, increases monotonically above 500 K, and exceeds the type B uncertainty at 800 K and above. The increase in total uncertainty is exclusively affected by the increase in the variance with temperature. This result implies variability from within the sample, possibly due to compositional inhomogeneity, rather than from the instrumentation. We note however, that the type A uncertainty component is very small (≈0.5 μV/K at 900 K) and is well within the uncertainty of most commercial and custom-built Seebeck coefficient instrumentation.

To characterize the thermocyclic evolution of the Seebeck coefficient, we next plot the Seebeck coefficient interpolated at specified temperatures as a function of the cycle number (Figure 3). The Seebeck coefficient data at higher temperature appears marginally noisier than at lower temperature, but are consistent within the type B uncertainty. Any cycle dependent drift in the Seebeck coefficient is then quantified by calculating the slope of the unconstrained linear fit of the data obtained for each temperature. The average drift in the Seebeck coefficient is ≈ − 21 nV/K per cycle and is negligible in comparison to the total measurement uncertainty. Based on this analysis, constantan exhibits moderate stability in the selected temperature range, at least below 800 K. However, the moderately high thermal conductivity (≈19.5 W/mK) of constantan may impose a practical limitation for measurement instrumentation designed to provide thermal gradient heater power to thermoelectric materials with specific (but low) thermal conductivity.

Figure 4(a) plots the Seebeck coefficient for SC-$Si_{90}Ge_{10}$ as a function of temperature for the complete set of 10 cycles, including the consensus mean curve, the type A expanded confidence intervals, and the total expanded uncertainty confidence bands. The expanded uncertainty is clearly larger for this material as compared to constantan and increases with temperature. As before, we first characterize the stability of SC-$Si_{90}Ge_{10}$ by comparing the distribution of the data (the type A component) with the type B component. Figure 4(b) plots the type A and type B uncertainty components as a function of temperature. In comparison to the type B uncertainty component (≈3 μV/K, or ≈0.7% relative uncertainty through the temperature range), the type A component increases rapidly above 600 K and exceeds the type B component near 700 K, rising to nearly 4× that of the type B component by 900 K. The increase in total uncertainty is clearly dominated by the increase in the variance with temperature.

We next plot the Seebeck coefficient interpolated at specified temperatures as a function of the cycle number (Figure 5). The Seebeck coefficient data at higher temperature is significantly noisier than at lower temperature. The cycle dependent drift in the Seebeck coefficient is then quantified by calculating the slope of the unconstrained linear fit

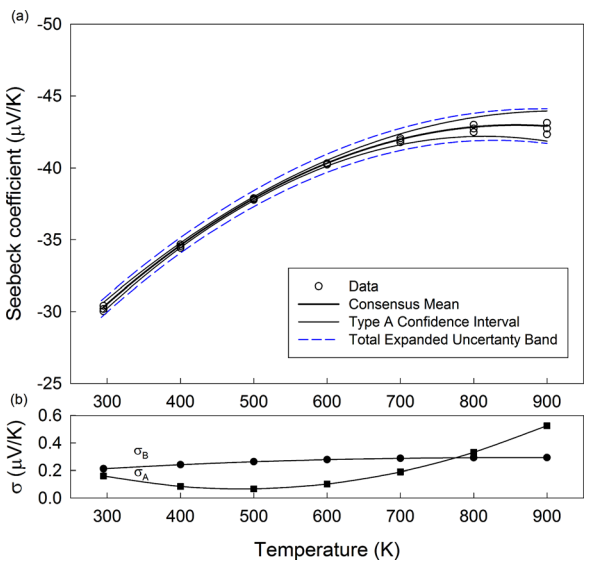

FIG. 2. (a) The Seebeck coefficient for constantan as a function of temperature for 10 cycles (open circles), including the consensus mean curve (dark solid black line), the type A expanded confidence intervals (light solid black line), and the total expanded uncertainty confidence bands (dashed blue lines); (b) the type A and type B uncertainty components (labeled as σ_A and σ_B, respectively) as a function of temperature.

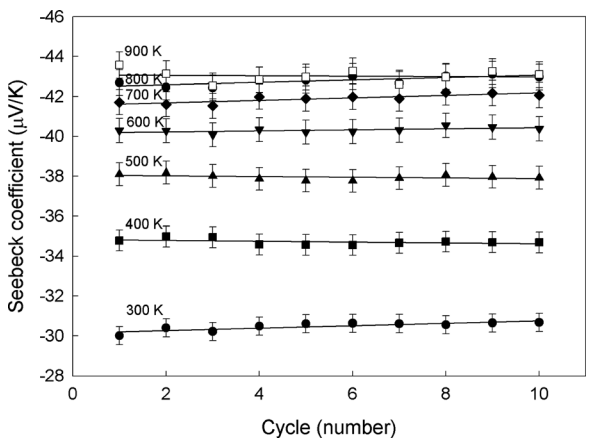

FIG. 3. The Seebeck coefficient for constantan interpolated at specified temperatures as a function of the cycle number. The solid lines are the slope of the unconstrained linear fit of the data obtained for each temperature and the error bars represent the type B uncertainty described in the analysis section. The symbols are shown in contrasting shapes and fillings for visual clarity.

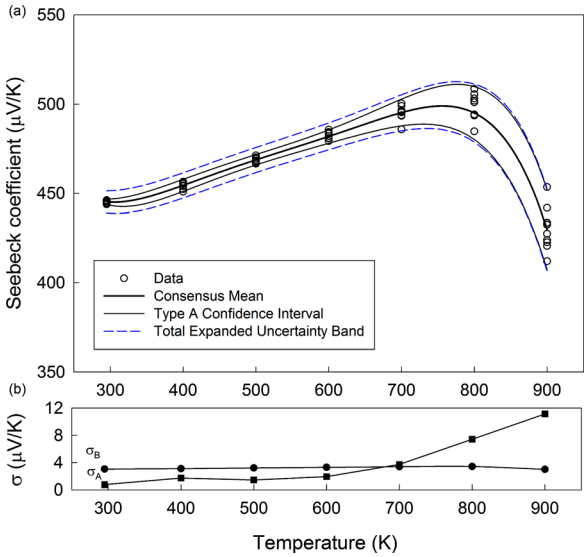

FIG. 4. (a) The Seebeck coefficient for SC-$Si_{90}Ge_{10}$ as a function of temperature for 10 cycles (open circles), including the consensus mean curve (dark solid black line), the type A expanded confidence intervals (light solid black line), and the total expanded uncertainty confidence bands (dashed blue lines); (b) the type A and type B uncertainty components (labeled as σ_A and σ_B, respectively) as a function of temperature.

of the data obtained for each temperature. The average drift in the Seebeck coefficient is ≈ -285 nV/K per cycle. Since the greatest rise in variance occurs in the intrinsic region (>800 K),[8] and the thermocyclic evolution of the Seebeck coefficient is more random than cumulative, we suspect the instability arises from silicon-germanium composition inhomogeneity, rather than from dopant precipitation. Thus, we determine that SC-$Si_{90}Ge_{10}$ does not exhibit the stability required for use as a SRM in this temperature range.

Finally, we present the Seebeck coefficient for poly-$Si_{80}Ge_{20}$ as a function of temperature for the complete set of 10 cycles, including the consensus mean curve, the type A expanded confidence intervals, and the total expanded uncertainty confidence bands (Figure 6(a)). To characterize the stability of this material, we first compare the distribution of

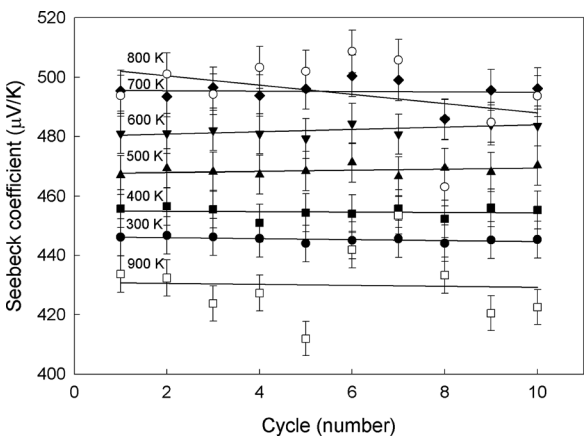

FIG. 5. The Seebeck coefficient for SC-$Si_{90}Ge_{10}$ interpolated at specified temperatures as a function of the cycle number. The solid lines are the slope of the unconstrained linear fit of the data obtained for each temperature and the error bars represent the type B uncertainty described in the analysis section. The symbols are shown in contrasting shapes and fillings for visual clarity.

the data (the type A component) with the type B component. The type A and type B uncertainty components are plotted in Figure 6(b) as a function of temperature. Throughout the temperature range, the type B relative uncertainty is ≈0.7%. The type A uncertainty component is continuous (≈0.6 μV/K, or ≈0.5% relative uncertainty) and smaller than the type B component throughout the entire temperature range–about 2.5× lower at 900 K.

To characterize the thermocyclic evolution of the Seebeck coefficient, we next plot the Seebeck coefficient interpolated at specified temperatures as a function of the cycle number (Figure 7). The Seebeck coefficient data are extremely consistent and within the type B uncertainty. The cycle dependent drift in the Seebeck coefficient is then quantified by calculating the slope of the unconstrained linear fit of the data obtained for each temperature. The drift in the Seebeck coefficient, ≈ -18 nV/K per cycle at 300 K with an average drift of ≈ -65 nV/K per cycle for the temperature range, is negligible in comparison to the total measurement uncertainty, ≈2 μV/K at 300 K. Furthermore, the direction of the drift is in the opposite direction as compared to the trends observed under long-term isothermal annealing, where the absolute Seebeck coefficient increases as a function of both annealing time and temperature.[12,13] Based on the above analysis, we determine that poly-$Si_{80}Ge_{20}$ exhibits extremely favorable stability in the selected temperature range.

As an additional evaluation of the thermocyclic stability, four-probe Hall measurements were conducted at 300 K on representative silicon germanium alloy samples (sliced using a wire saw into the approximate dimensions 0.5 mm × 2 mm × 8 mm) using the Quantum Design PPMS infrastructure and a custom measurement sequence. Samples were measured before the first thermal cycle, then after the 5th and 10th thermal cycle, cycled in place with the SC-$Si_{90}Ge_{10}$ thermocyclic series. The Hall resistance, R_H, was measured as a function

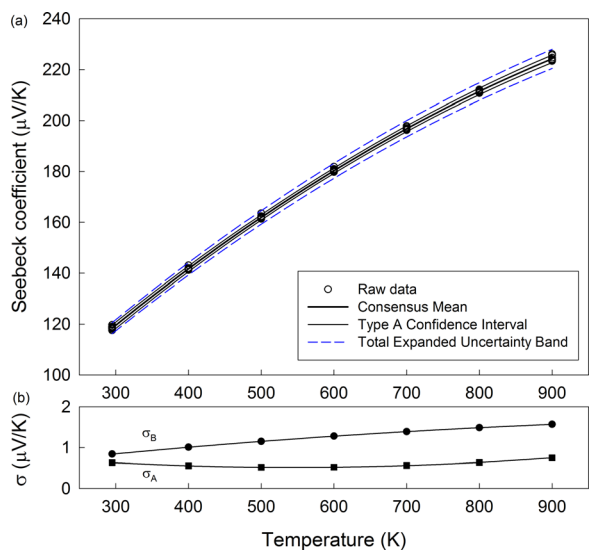

FIG. 6. (a) The Seebeck coefficient for poly-$Si_{80}Ge_{20}$ as a function of temperature for 10 cycles (open circles), including the consensus mean curve (dark solid black line), the type A expanded confidence intervals (light solid black line), and the total expanded uncertainty confidence bands (dashed blue lines); (b) the type A and type B uncertainty components (labeled as σ_A and σ_B, respectively) as a function of temperature.

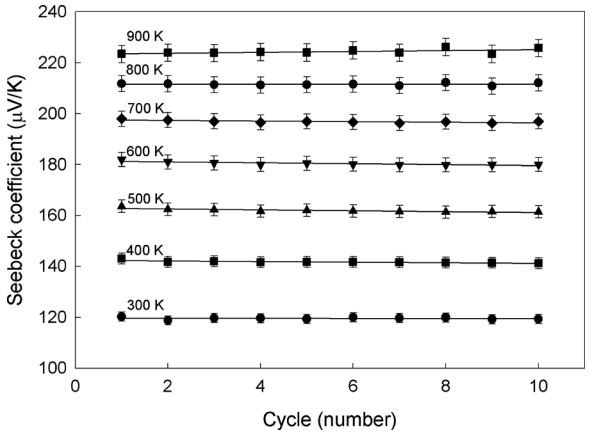

FIG. 7. The Seebeck coefficient for poly-$Si_{80}Ge_{20}$ interpolated at specified temperatures as a function of the cycle number. The solid lines are the slope of the unconstrained linear fit of the data obtained for each temperature and the error bars represent the type B uncertainty described in the analysis section. The symbols are shown in contrasting shapes for visual clarity.

TABLE I. Carrier concentration (cm^{-3}) at 300 K measured on representative silicon germanium alloy samples as a function of thermal cycles.

	0 Cycles	5 Cycles	10 Cycles
SC-$Si_{90}Ge_{10}$	3.66×10^{18}	3.26×10^{18}	3.37×10^{18}
poly-$Si_{80}Ge_{20}$	1.71×10^{20}	1.81×10^{20}	1.75×10^{20}

of multiple positive and negative magnetic fields ($-2.5\,T < B < 2.5\,T$) to mitigate voltage probe misalignment effects and thermal instabilities. R_H values for matching $\pm B$ were averaged using multiple zero field measurements. The carrier concentration was calculated for each sample using the relation $n = 1/[(R_H/B)(et)]$,[20] where R_H/B is the unconstrained-intercept fitted slope for the collection of R_H and B values, n the carrier concentration, e the charge per carrier, and t the sample thickness. These carrier concentration values are listed in Table I. Prior to any thermal cycling, the carrier concentration for the SC-$Si_{90}Ge_{10}$ sample was $3.66 \times 10^{18}\,cm^{-3}$ and $1.71 \times 10^{20}\,cm^{-3}$ for the poly-$Si_{80}Ge_{20}$ sample; after the 10th cycle, the carrier concentration for the SC-$Si_{90}Ge_{10}$ sample was $3.37 \times 10^{18}\,cm^{-3}$ and $1.75 \times 10^{20}\,cm^{-3}$ for the poly-$Si_{80}Ge_{20}$ sample. The carrier concentrations were invariant as a function of the thermal cycle for both materials within the measurement uncertainty (5%).

CONCLUSION

We have characterized the thermocyclic variability of the Seebeck coefficient by measuring the temperature dependence of the Seebeck coefficient as a function of 10 sequential thermal cycles and by employing multiple regression analysis for the selected candidate materials: constantan, p-type single crystal SiGe, and p-type polycrystalline SiGe. Constantan exhibits moderate stability but at somewhat lower temperature than the desired range for the SRM. The temperature independence and magnitude of the electrical resistivity might not be desirable if resistivity is included as supplemental data with the Seebeck coefficient SRM. In addition, the moderately high thermal conductivity (≈19.5 W/mK) of constantan may, in some cases, impose a practical limitation for measurement instrumentation designed to provide thermal gradient heater power to thermoelectric materials with specific (but low) thermal conductivity. For SC-$Si_{90}Ge_{10}$, the measured variance increases rapidly with temperature and exceeds the instrumentation uncertainty near 700 K, rising to nearly 4× that of the type B component by 900 K. At any specified temperature, the Seebeck coefficient from cycle to cycle shows large variation. SC-$Si_{90}Ge_{10}$ does not exhibit the stability required for use as a SRM in this temperature range. For poly-$Si_{80}Ge_{20}$, the variance is nearly continuous much and smaller than the instrumentation uncertainty throughout the entire temperature range, about 2.5× lower at 900 K. Based on our analysis, poly-$Si_{80}Ge_{20}$ exhibits extremely favorable stability in the selected temperature range. In addition, the electrical resistivity and thermal conductivity values are both suitable for immediate use in custom and commercial instrumentation designed for measurements on thermoelectric materials.

[1]G. S. Nolas, J. Sharp, and H. J. Goldsmid, *Thermoelectrics: Basic Principles and New Materials Developments* (Springer, New York, NY, 2001).
[2]*Thermoelectrics Handbook*, edited by D. M. Rowe (CRC Press, Boca Raton, FL, 1995).
[3]J. Martin, T. Tritt, and C. Uher, J. Appl. Phys. **108**, 121101 (2010).
[4]T. M. Tritt, in *Thermoelectrics Handbook: Macro to Nano* (CRC Press, Boca Raton, FL, 2005), p. 23.
[5]J. Martin, Meas. Sci. Technol. **24**, 085601 (2013).
[6]N. D. Lowhorn, W. Wong-Ng, Z-Q. Lu, J. Martin, M. L. Green, J. E. Bonevich, and E. L. Thomas, J. Mater. Res. **26**, 1983 (2011).
[7]Certain commercial equipment, instruments, or materials are identified in this document. Such identification does not imply recommendation or endorsement by the National Institute of Standards and Technology, nor does it imply that the products identified are necessarily the best available for the purpose.
[8]T. Akashi, I. Yonenaga, I. Gunjishima, and T. Goto, Mater. Trans. **42**, 1024 (2001).
[9]R. Bentley, *Theory and Practice of Thermoelectric Thermometry* (Springer-Verlag Singapore Pte. Ltd., Singapore 1998), p. 70.
[10]V. S. Shukla and D. M. Rowe, Phys. Status Solidi **66**, 243 (1981).
[11]I. M. Lifshitz and V. V. Slyozov, J. Phys. Chem. Solids **19**, 35 (1961).
[12]R. D. Nasby and E. L. Burgess, J. Appl. Phys. **43**, 2908 (1972).
[13]V. Raag, in *Proc. Intersociety Energy Conversion Engineering Conf.* (IEEE, New York, 1975), p. 723.
[14]D. M. Rowe and N. Savvides, J. Phys. D: Appl. Phys. **12**, 1613 (1979).
[15]J. P. Dismukes, L. Ekstrom, E. F. Steigmeier, I. Kudman, and D. S. Beers, J. Appl. Phys. **35**, 2899 (1964).
[16]J. Martin, Rev. Sci. Instrum. **83**, 065101 (2012).
[17]Z. Q. J. Lu, N. D. Lowhorn, W. Wong-Ng, W. Zhang, E. L. Thomas, M. Otani, M. L. Green, T. N. Tran, C. Caylor, N. R. Dilley, A. Downey, B. Edwards, N. Elsner, S. Ghamaty, T. Hogan, Q. Jie, Q. Li, J. Martin, G. Nolas, H. Obara, J. Sharp, R. Venkatasubramanian, R. Willigan, J. Yang, and T. Tritt, J. Res. Natl. Inst Stand. Technol. **114**, 37 (2009).
[18]JCGM 100:2008, *Evaluation of Measurement Data-Guide to the Expression of Uncertainty in Measurement* (ISO GUM 1995 with minor corrections) (Joint Committee for Guides in Metrology, 2008).
[19]B. N. Taylor and C. E. Kuyatt, *Guidelines for Evaluating and Expressing Uncertainty of NIST Measurement Results*, NIST Technical Note 1297 (U.S. Government Printing Office, Washington, DC, 1994), Available at http://www.nist.gov/pml/pubs/tn1297/index.cfm.
[20]C. Kittel, *Solid State Physics,* 2nd ed. (John Wiley & Sons, Inc., New York, 1956), p. 296.